Electrocatalysis

Deutsche Ausgabe: DOI: 10.1002/ange.201511032
Internationale Ausgabe: DOI: 10.1002/anie.201511032

Strong-Coupled Cobalt Borate Nanosheets/Graphene Hybrid as Electrocatalyst for Water Oxidation Under Both Alkaline and Neutral Conditions

Pengzuo Chen[+], Kun Xu[+], Tianpei Zhou, Yun Tong, Junchi Wu, Han Cheng, Xiuli Lu, Hui Ding, Changzheng Wu, and Yi Xie*

Abstract: *Developing highly active catalysts for the oxygen evolution reaction (OER) is of paramount importance for designing various renewable energy storage and conversion devices. Herein, we report the synthesis of a category of Co-Pi analogue, namely cobalt-based borate (Co-B_i) ultrathin nanosheets/graphene hybrid by a room-temperature synthesis approach. Benefiting from the high surface active sites exposure yield, enhanced electron transfer capacity, and strong synergetic coupled effect, this Co-B_i NS/G hybrid shows high catalytic activity with current density of 10 mA cm^{-2} at overpotential of 290 mV and Tafel slope of 53 mV dec^{-1} in alkaline medium. Moreover, Co-B_i NS/G electrocatalysts also exhibit promising performance under neutral conditions, with a low onset potential of 235 mV and high current density of 14.4 mA cm^{-2} at 1.8 V, which is the best OER performance among well-developed Co-based OER electrocatalysts to date. Our finding paves a way to develop highly active OER electrocatalysts.*

The increasing environmental problem and energy crisis has sparked a mass of research efforts in exploring alternative energy storage and conversion system.[1] Hydrogen has been regarded as a clean alternative energy owing to the high energy output and green combustion products.[2] Electrochemical water splitting is a promising technology to convert electric energy into chemical fuels stored by hydrogen.[3] However, the overall water splitting efficiency is greatly impeded by the oxygen evolution reaction (OER) owing to the sluggish kinetics derived from a multistep proton-coupled electron transfer process.[4] For this reason, many electrocatalysts have been explored to lower the requirement of overpotential and expedite the OER reaction kinetics process, and thereby improve the efficiency of water oxidation.[5] To date, the most active OER electrocatalysts are noble metal oxides (RuO_2 or IrO_2), but their large-scale application has been greatly hindered because of their high cost and scarcity.[6] Therefore, it is highly desirable to develop effective non-noble metal OER electrocatalysts to enhance the energy conversion efficiency of water oxidation.

In nature, the oxygen-evolving complex (OEC) that consists of manganese and calcium is well known as a water splitting complex.[7] Biomimetically, a new category of artificial water oxidation electrocatalysts with amorphous features composed of cobalt, oxygen, and inorganic phosphate, namely cobalt–phosphate (Co-P_i) OEC, have attracted significant attention owing to its low cost, self-repair mechanism, high intrinsic activity, and superior stability.[8] For example, an amorphous Janus nanoparticulate cobalt–oxide film (O_2-CoCat) electrocatalyst formed by electrodeposition exhibits enhanced electrocatalytic performance.[9] Moreover, nanostructured cobalt metaphosphate ($Co(PO_3)_2$) materials prepared by the thermolytic molecular precursor approach shows low onset potentials and comparable turnover frequency in neutral conditions.[10] However, the low surface active site exposure yield and time-consuming synthesis process greatly limited the large-scale practical application of Co-P_i electrocatalysts for OER.

Two-dimensional (2D) ultrathin nanosheets, as promising structure motif for OER, have attracted remarkable attention owing to the realization of synergetic improvement of active surface area and intimate contact with support electrodes.[11] Meanwhile, graphene sheets, as accessible 2D materials with high electrical conductivity, not only can enhance the electron transfer but also provide a desired support to protect the in situ growth of nanosheets from agglomeration.[12] In this regard, developing a new category of Co-P_i analogue/graphene hybrid with 2D ultrathin morphology is highly desirable for water oxidation. Herein, we report a room-temperature chemical route to design a Co-P_i analogue, namely amorphous Co-B_i ultrathin nanosheet/graphene hybrid (denoted as Co-B_i NS/G), as a highly active OER electrocatalyst both in alkaline and neutral media. Benefiting from the high exposed surface active sites, enhance electron transfer capacity and strong synergetic coupled effects, Co-B_i NS/G hybrids exhibit highly efficient OER electrocatalytic activity with overpotential of 290 mV at a current density of 10 mA cm^{-2} and Tafel slope around 53 mV dec^{-1} in alkaline medium. Furthermore, this Co-B_i NS/G hybrid achieves a very low onset potential of 235 mV and high current density value of 14.4 mA cm^{-2} at 1.8 V versus RHE under neutral

[*] P. Z. Chen,[+] K. Xu,[+] T. P. Zhou, Y. Tong, J. C. Wu, H. Cheng, X. L. Lu, H. Ding, Prof. C. Z. Wu, Prof. Y. Xie
School of Chemistry and Materials Science
State Key Laboratory of Fire Science (SKLFS)
iChEM (Collaborative Innovation Center of Chemistry for Energy Materials)
CAS Center for Excellence in Nanoscience and
CAS Key Laboratory of Mechanical Behavior and Design of Materials
University of Science and Technology of China
Hefei, Anhui 230026 (P. R. China))
E-mail: czwu@ustc.edu.cn

[+] These authors contributed equally to this work.

Supporting information for this article is available on the WWW under http://dx.doi.org/10.1002/anie.201511032.

condition, which is the best performance among reported cobalt-based OER electrocatalysts to date.

In this study, the amorphous Co-B_i ultrathin nanosheet/graphene hybrid was synthesized by a facile chemical synthesis method at room temperature (Scheme 1). The mor-

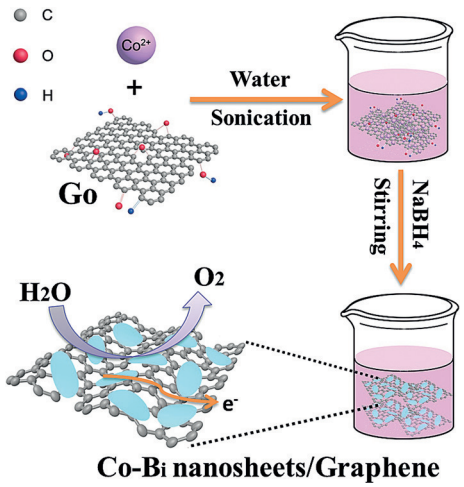

Scheme 1. The synthesis of Co-B_i nanosheets grown in situ on graphene sheets at room temperature.

phology and composition were first evaluated by the field emission scanning electron microscopy (FE-SEM) and the transmission electron microscopy (TEM). As shown in Figure 1 a–c and Figure S5, the SEM images of as-prepared Co-B_i NS/G product exhibit uniform nanosheet morphology with a lateral size of several micrometers and further TEM images confirm the existence of small nanosheets grown on graphene (Figure 1 d,e). In contrast, the SEM and TEM images of the simple Co-B_i product shows a hierarchical structure comprised of aggregated ultrathin nanosheets (Supporting Information, Figure S6,7). Moreover, in Figure 1 f, the EDS mapping characterizations demonstrated the homogenous distribution of Co (purple), B (green), O (blue) and C (red) in the as-prepared Co-B_i NS/G product.

The structure information of Co-B_i NS/G hybrids and simple Co-B_i product were further investigated by X-ray diffraction (XRD) and Raman spectrum. As shown in Figure 2 a, the XRD pattern of Co-B_i NS/G hybrids exhibit only one peak of graphene, indicating an amorphous structure Co-B_i ultrathin nanosheets. Moreover, the Raman spectra analysis gives further evidence for the amorphous character of Co-B_i nanosheets. As shown in Figure 2 b, there are no characteristic peaks of Co-B_i, and only two prominent bands located at 1590 cm^{-1} and 1350 cm^{-1} that correspond to the vibration of sp^2-bonded carbon atoms and the dispersive, defect-induced vibrations, respectively, revealing amorphous character for the Co-B_i product (Figure S3, S4).[13] Further information on the composition and valence state of the samples was obtained by X-ray photoelectron spectroscopy (XPS). Figure S9a shows the survey XPS spectrum, which clearly indicated that the sample consists of Co, B, O, and C. The high-resolution core spectrum of Co 2p is shown in Figure 2 c, the peak at 781.4 and 797.2 eV core levels are

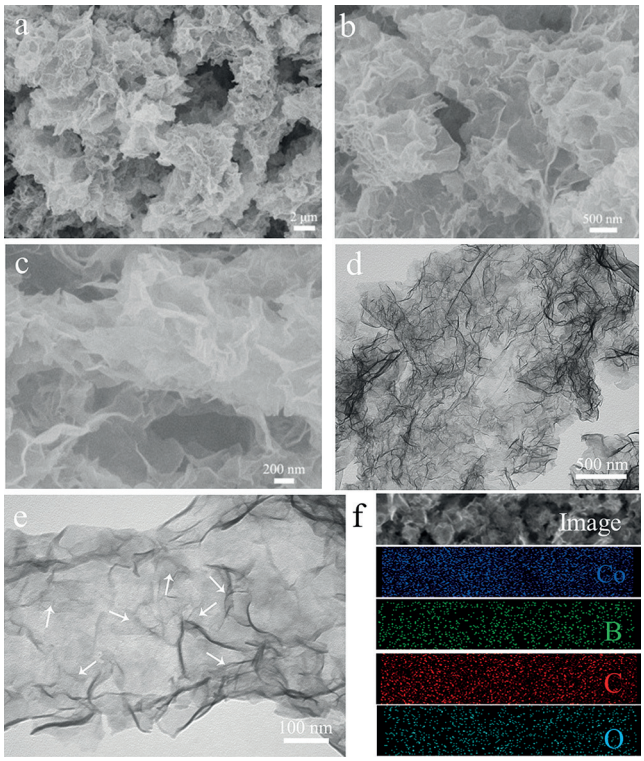

Figure 1. a,b) The low-resolution and c) high-resolution SEM images of Co-B_i NS/G product. d) The low-resolution and e) high-resolution TEM images of Co-B_i NS/G product (white arrows point at some Co-B_i nanosheets). f) The EDS mapping images of as-prepared Co-B_i NS/G product.

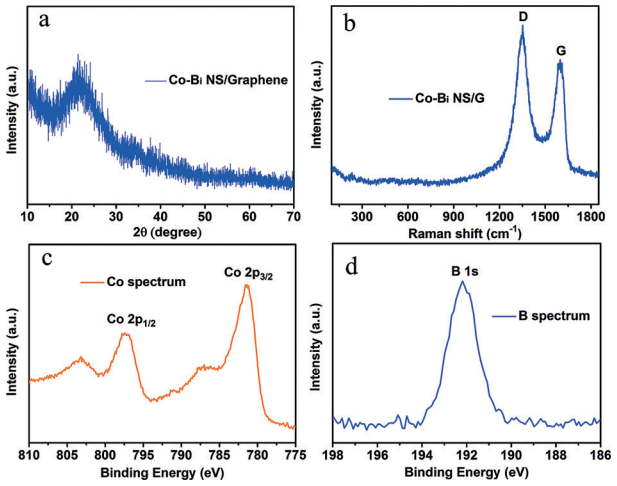

Figure 2. a) XRD pattern and b) Raman spectrum of Co-B_i NS/G product. c) Co_{2p} and d) B_{1s} core levels spectra of Co-B_i NS/G product.

observed, which is consistent with the Co^{2+} of the as-prepared Co-B_i electrocatalyst.[14] In the B regions, a sharp characteristic peaks with 192.1 eV binding energy, which can be assigned to the 1s core levels of B^{3+} in borate species (Figure 2 d and Figure S11b).[15] Moreover, a peak at the binding energy of 531.7 eV can be ascribed to the O_{1s} signals (Figure 2 e).[14] The resulting Co/B/O ratios of Co-B_i NS/G are ca. 1.47:1:4.16, which can further be achieved by calculated

from the XPS data. Therefore, the structural formula of as-prepared Co-B_i product can be approximately formulated as $Co_3B_2O_6$, since it is rational for considering adsorbed oxygen on the surface. Based on the above results, the Co-B_i nanosheets/graphene hybrid material has been developed successfully, which provides a new opportunity to investigate the OER catalytic activity of cobalt-based borate compounds.

To investigate OER electrocatalytic activities of the as-prepared Co-B_i NS/G catalysts, the samples were first deposited onto glass carbon electrodes (GCE) to form a uniform catalyst film with a catalyst loading of 0.285 mg cm^{-2}. Moreover, a commercial RuO_2 catalyst was also used as a standard value to accurately evaluate their OER activities. Polarization curves were recorded from linear sweep voltammetry (LSV) tests with a scan rate of 5 mV s^{-1} in O_2-saturated 1 M KOH solution. In Figure 3a, the OER polarization curves of Co-B_i NS/G achieves a current density of 10 mA cm^{-2} at a low overpotential of 290 mV, whereas a higher overpotential of 305 mV and 345 mV is required for the RuO_2 and Co-B_i catalysts, respectively. The corresponding Tafel slope of Co-B_i NS/G in Figure 2b was measured to be 53 mV dec^{-1}, which is smaller than that of the Co-B_i sample (72 mV dec^{-1}). This result suggests the improved OER reaction kinetics because of the enhanced electron transfer capacity and strong coupled effects. In addition, both the long-term CV cycling test and time-dependent current density curves provide direct evidence of the superior stability of as-prepared Co-B_i NS/G in alkaline medium (Figure S11 and Figure 3c). To further understand the kinetics during the OER process, electrochemical impedance spectroscopy (EIS) has been performed in 1 M KOH solution. As shown in Figure 3d, the Nyquist plots reveal that the charge transfer resistance (12.3 Ω) of Co-B_i NS/G catalyst is obviously lower than that of simple Co-B_i catalyst (35.7 Ω), suggesting Co-B_i NS/G hybrid catalyst possesses the faster charge transfer process.

To further understand the reaction mechanism, the rotating ring-disk electrode (RRDE) has been used to analyze the content of by-product (peroxide intermediates) that formed at the surface of Co-B_i NS/G catalyst during the OER process. Figure 3e shows a relatively low ring current value (black curve), which is far lower than that of the disk current (purple curve), indicating negligible hydrogen peroxide formation. Additionally, the ring current gradually decreases from low potential to high potential, suggesting that fewer peroxide intermediates formed at the high potential region. This result indicates that the rapid increase of current density can be mainly attributed to a desirable four-electron transfer pathway to form O_2 for the OER process (Figure 3e). Furthermore, a Faradaic efficiency test was performed to verify the rapid increase of current density is originating from water oxidation rather than from side reactions. First, an RRDE with a ring electrode is used to carry out a continuous OER (disk electrode)-ORR (ring eletrode) process. The disk current is fixed at a potential range from 150 μA to 320 μA to generate O_2 molecules from the Co-B_i NS/G catalyst, and then the O_2 molecules are further reduced by sweeping across the surrounding Pt ring electrode with an ORR potential of 0.45 V versus RHE. As shown in Figure 3f, the collected ring current is approximately 52.7 μA when the applied disk current is fixed at 150 μA, corresponding to a Faradaic efficiency of 95.1 %. This result confirms the Co-B_i NS/G catalyst could provide fast 4-electron reaction to generate O_2 molecules at relatively low potential. Moreover, a steady ring current of 117.4 μA can be further observed under higher applied disk current (320 μA). The corresponding Faradaic efficiency of 99.2 % indicates the detected oxidation current catalyzed by Co-B_i NS/G catalyst can be ascribed to oxygen evolution reaction process.[16] Meanwhile, Figure 3g shows the relationship between Faradaic efficiency and applied potential, confirming that Faradaic efficiency increases with the rising potential. This

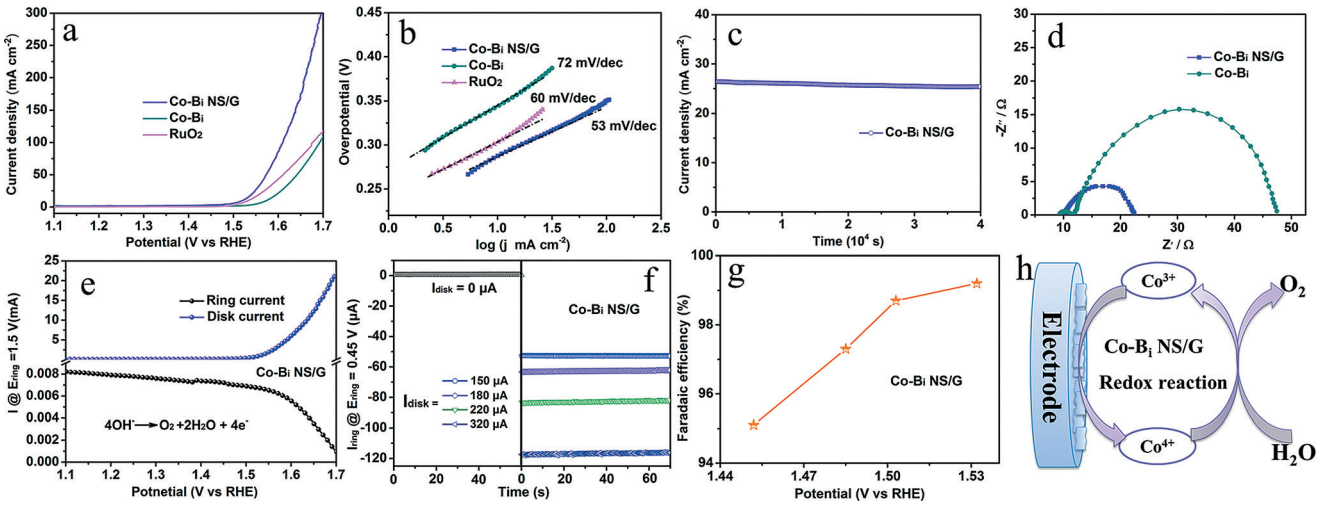

Figure 3. a) Polarization curves and b) corresponding Tafel plots of Co-B_i NS/G, simple Co-B_i and commercial RuO_2 catalysts in 1 M KOH solution. c) Chronoamperometric response of Co-B_i NS/G and d) EIS spectrum of as-prepared samples recorded at a constant potential of 1.55 V vs. RHE. e) Disk and ring current of Co-B_i NS/G catalyst on an RRDE (1600 rpm) with a ring potential of 1.5 V in 1 M KOH solution. f) Ring current of Co-B_i NS/G catalyst on an RRDE (1600 rpm) with a ring potential of 0.45 V in 1 M KOH solution at different disk current. g) The plot of Faradaic efficiency of Co-B_i NS/G electrocatalyst at different disk potential in 1 M KOH solution. h) Proposed process for Co-B_i NS/G as redox catalysts for water oxidation.

result suggests the higher valence state of Co^{4+} is actually the main active center for the water oxidation reaction, indicating that our OER catalytic mechanism is consistent with previously reported results.[17] As shown in Figure 3h, the current density will rapidly rise when the potential beyond the $Co^{4+/3+}$ redox couple, reflecting the electrochemical generation of Co^{4+} states in Co-B_i NS/G that act as redox active centers for the water oxidation in the recycling of Co states. Therefore, above electrochemical test results confirm that Co-B_i NS/G catalyst is a promising electrode material for water oxidation in alkaline medium.

Exploring high efficiency OER electrocatalysts under neutral condition is of great significance because of the consideration of safety and cost for water splitting electrolyzer. Over the past few years, many efforts have been devoted to develop highly active cobalt-based OER electrocatalysts in neutral medium.[18] However, the relative low current density and overpotential is still far from the requirement of practical applications. This novel cobalt-based borate (Co-B_i)/graphene hybrid electrocatalyst is also expected to be a promising candidate for high-performance OER electrocatalyst in neutral solution. For this purpose, the OER performance of Co-B_i NS/G catalyst was further investigated in phosphate buffer solution (pH 7.0). As shown in Figure 4a,

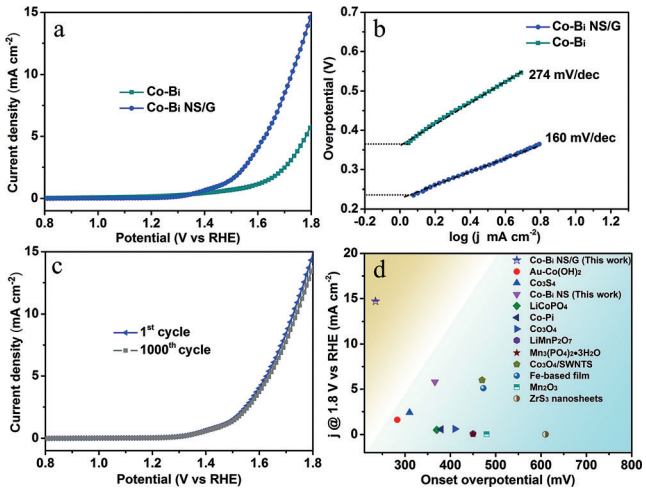

Figure 4. a) Polarization curves and b) corresponding Tafel plots of Co-B_i NS/G and simple Co-B_i catalysts in neutral medium. c) Polarization curves of Co-B_i NS/G before and after CV testing of 1000 cycles in neutral medium. d) The onset overpotential and current density of well-developed OER electrocatalysts at a potential of 1.8 V vs. RHE in neutral solution (Table S2).

Co-B_i NS/G catalyst exhibits an exceptional small onset overpotential of 235 mV for catalytic O_2 formation, and achieves a high current density of 14.4 mA cm^{-2} at potential of 1.8 V versus RHE, which is superior to most cobalt-based electrocatalysts under neutral condition (Table S2). Moreover, benefiting from the highly exposed surface active sites, enhanced electron transfer capacity, and strong synergistic coupled effects, Co-B_i NS/G catalyst shows an obvious reduced Tafel slope of 160 mV dec^{-1} compared with simple Co-B_i catalyst (274 mV dec^{-1}). Besides OER activity, the durability in neutral solutions has also been evaluated. As shown in Figure 4c, the Co-B_i NS/G catalyst displayed negligible degeneration of current density after 1000 CV cycling tests, and the current density of Co-B_i NS/G catalyst remained stable at a potential of 1.65 V versus RHE for 60000 s (Figure S12), demonstrating the high stabilities of Co-B_i NS/G materials for the OER process in neutral medium.

Based on the above experimental results, an amorphous cobalt-based borate ultrathin nanosheet was grown in situ on graphene sheets, and was established as an active OER electrocatalyst. This Co-B_i NS/G hybrid catalyst not only exhibits superior OER catalytic activity under alkaline condition, but could also be performed in neutral medium. The high OER catalytic activity of the Co-B_i NS/G hybrid catalyst can be attributed to the following aspects: 1) The high intrinsic OER catalytic activity of Co-B_i amorphous materials. 2) The specific 2D ultrathin nanosheet structure can expose more active surface area to offer more active sites for water oxidation. 3) Graphene nanosheet supports can expedite electron transfer to improve the OER kinetics processes. 4) The strong synergistic coupled effects between Co-B_i nanosheets and graphene support assisted in improving charge transport, and thus lead to superior OER performance. Therefore, these collaborative advantages endow the Co-B_i NS/G electrocatalyst with superior OER catalytic activity.

In conclusion, we have successfully fabricated a Co-Pi analogue, namely amorphous Co-based borate ultrathin nanosheet/graphene hybrid (denote as Co-B_i NS/G) by a room-temperature chemical approach, and investigated it as an OER electrocatalyst for the first time. Benefiting from the high surface active sties exposure yield, enhanced electron transfer capacity, and strong synergistic coupled effects, the Co-B_i NS/G hybrid electrocatalyst shows high OER catalytic active and superior stability in both alkaline and neutral solutions. This work not only offers a facile and mild method to synthesize cobalt-based electrocatalysts, but also experimentally demonstrates the potential applications of this new Co-B_i nanosheet in water oxidation, paving a new way to develop highly active OER electrocatalysts.

Acknowledgements

This work was financially supported by the National Basic Research Program of China (2015CB932302), the Natural Science Foundation of China (21222101, U1432133, 11132009, 21331005, 11321503, J1030412), the Chinese Academy of Science (XDB01020300), the Fok Ying-Tong Education Foundation, China (Grant No.141042),the China Postdoctoral Science Foundation (No. 2015M580539) and the Fundamental Research Funds for the Central Universities (WK2060190027).

Keywords: amorphous materials · cobalt–borate · hybrids · nanosheets · oxygen evolution reaction

How to cite: *Angew. Chem. Int. Ed.* **2016**, *55*, 2488–2492
Angew. Chem. **2016**, *128*, 2534–2538

[1] a) X. Huang, Z. Zeng, H. Zhang, *Chem. Soc. Rev.* **2013**, *42*, 1934 – 1946; b) T. R. Cook, D. K. Dogutan, S. Y. Reece, Y. Surendranath, T. S. Teets, D. G. Nocera, *Chem. Rev.* **2010**, *110*, 6474 – 6502.
[2] a) L. Hammarström, S. Hammes-Schiffer, *Acc. Chem. Res.* **2009**, *42*, 1859 – 1860; b) R. F. Service, *Science* **2009**, *324*, 1257 – 1259.
[3] a) J. Chen, X.-J. Wu, L. Yin, B. Li, X. Hong, Z. Fan, B. Chen, C. Xue, H. Zhang, *Angew. Chem. Int. Ed.* **2015**, *54*, 1210 – 1214; *Angew. Chem.* **2015**, *127*, 1226 – 1230; b) X.-J. Wu, X. Huang, X. Qi, H. Li, B. Li, H. Zhang, *Angew. Chem. Int. Ed.* **2014**, *53*, 8929 – 8933; *Angew. Chem.* **2014**, *126*, 9075 – 9079; c) Z. Zeng, C. Tan, X. Huang, S. Bao, H. Zhang, *Energy Environ. Sci.* **2014**, *7*, 797 – 803; d) W. Zhou, J. Zhou, Y. Zhou, J. Lu, K. Zhou, L. Yang, Z. Tang, L. Li, S. Chen, *Chem. Mater.* **2015**, *27*, 2026 – 2032; e) Z. Yin, B. Chen, M. Bosman, X. Cao, J. Chen, B. Zheng, H. Zhang, *Small* **2014**, *10*, 3537 – 3543.
[4] a) W. Zhou, X.-J. Wu, X. Cao, X. Huang, C. Tan, J. Tian, H. Liu, J. Wang, H. Zhang, *Energy Environ. Sci.* **2013**, *6*, 2921 – 2924; b) J. Suntivich, K. J. May, H. A. Gasteiger, J. B. Goodenough, Y. Shao-Horn, *Science* **2011**, *334*, 1383 – 1385; c) P. Chen, K. Xu, Y. Tong, X. Li, S. Tao, Z. Fang, W. Chu, X. Wu, C. Wu, *Inorg. Chem. Front.* **2015**, DOI: 10.1039/C5QI00197H; d) D. K. Bediako, Y. Surendranath, D. G. Nocera, *J. Am. Chem. Soc.* **2013**, *135*, 3662 – 3674; e) D. K. Bediako, B. Lassalle-Kaiser, Y. Surendranath, J. Yano, V. K. Yachandra, D. G. Nocera, *J. Am. Chem. Soc.* **2012**, *134*, 6801 – 6809.
[5] a) P. Chen, K. Xu, Z. Fang, Y. Tong, J. Wu, X. Lu, X. Peng, H. Ding, C. Wu, Y. Xie, *Angew. Chem. Int. Ed.* **2015**, *54*, 14710 – 14714; *Angew. Chem.* **2015**, *127*, 14923 – 14927; b) X. Long, G. Li, Z. Wang, H. Zhu, T. Zhang, S. Xiao, W. Guo, S. Yang, *J. Am. Chem. Soc.* **2015**, *137*, 11900 – 11903; c) L.-A. Stern, L. Feng, F. Song, X. Hu, *Energy Environ. Sci.* **2015**, *8*, 2347 – 2351; d) Y. Guo, Y. Tong, P. Chen, K. Xu, J. Zhao, Y. Lin, W. Chu, Z. Peng, C. Wu, Y. Xie, *Adv. Mater.* **2015**, *27*, 5989 – 5994.
[6] F. Li, B. Zhang, X. Li, Y. Jiang, L. Chen, Y. Li, L. Sun, *Angew. Chem. Int. Ed.* **2011**, *50*, 12276 – 12279; *Angew. Chem.* **2011**, *123*, 12484 – 12487.
[7] D. G. Nocera, *Acc. Chem. Res.* **2012**, *45*, 767 – 776.
[8] a) D. A. Lutterman, Y. Surendranath, D. G. Nocera, *J. Am. Chem. Soc.* **2009**, *131*, 3838 – 3839; b) R. S. Khnayzer, M. W. Mara, J. Huang, M. L. Shelby, L. X. Chen, F. N. Castellano, *ACS Catal.* **2012**, *2*, 2150 – 2160; c) N. Jiang, B. You, M. Sheng, Y. Sun, *Angew. Chem. Int. Ed.* **2015**, *54*, 6251 – 6254; *Angew. Chem.* **2015**, *127*, 6349 – 6352.
[9] S. Cobo, J. Heidkamp, P.-A. Jacques, J. Fize, V. Fourmond, L. Guetaz, B. Jousselme, V. Ivanova, H. Dau, S. Palacin, M. Fontecave, V. Artero, *Nat. Mater.* **2012**, *11*, 802 – 807.
[10] H. S. Ahn, T. D. Tilley, *Adv. Funct. Mater.* **2013**, *23*, 227 – 233.
[11] a) K. Xu, P. Chen, X. Li, Y. Tong, H. Ding, X. Wu, W. Chu, Z. Peng, C. Wu, Y. Xie, *J. Am. Chem. Soc.* **2015**, *137*, 4119 – 4125; b) X.-J. Wu, X. Huang, J. Liu, H. Li, J. Yang, B. Li, W. Huang, H. Zhang, *Angew. Chem. Int. Ed.* **2014**, *53*, 5083 – 5087; *Angew. Chem.* **2014**, *126*, 5183 – 5187; c) M. Chhowalla, H. S. Shin, G. Eda, L.-J. Li, K. P. Loh, H. Zhang, *Nat. Chem.* **2013**, *5*, 263 – 275; d) C. Tan, Z. Zeng, X. Huang, X. Rui, X.-J. Wu, B. Li, Z. Luo, J. Chen, B. Chen, Q. Yan, H. Zhang, *Angew. Chem. Int. Ed.* **2015**, *54*, 1841 – 1845; *Angew. Chem.* **2015**, *127*, 1861 – 1865; e) D. Yang, Z. Lu, X. Rui, X. Huang, H. Li, J. Zhu, W. Zhang, Y. M. Lam, H. H. Hng, H. Zhang, Q. Yan, *J. Am. Chem. Soc.* **2014**, *136*, 9352 – 9355.
[12] a) X. Long, J. Li, S. Xiao, K. Yan, Z. Wang, H. Chen, S. Yang, *Angew. Chem. Int. Ed.* **2014**, *53*, 7584 – 7588; *Angew. Chem.* **2014**, *126*, 7714 – 7718; b) J. Yang, D. Voiry, S. J. Ahn, D. Kang, A. Y. Kim, M. Chhowalla, H. S. Shin, *Angew. Chem. Int. Ed.* **2013**, *52*, 13751 – 13754; *Angew. Chem.* **2013**, *125*, 13996 – 13999.
[13] V. Chandra, K. S. Kim, *Chem. Commun.* **2011**, *47*, 3942 – 3944.
[14] a) S. S. Muir, Z. Chen, B. J. Wood, L. Wang, G. Q. Lu, X. Yao, *Int. J. Hydrogen Energy* **2014**, *39*, 414 – 425; b) C. Wu, Y. Bai, D.-X. Liu, F. Wu, M.-L. Pang, B.-L. Yi, *Catal. Today* **2011**, *170*, 33 – 39.
[15] a) M. Dincă, Y. Surendranath, D. G. Nocera, *Proc. Natl. Acad. Sci. USA* **2010**, *107*, 10337 – 10341; b) N. Patel, R. Fernandes, G. Guella, A. Kale, A. Miotello, B. Patton, C. Zanchetta, *J. Phys. Chem. C* **2008**, *112*, 6968 – 6976.
[16] a) T. Y. Ma, S. Dai, M. Jaroniec, S. Z. Qiao, *J. Am. Chem. Soc.* **2014**, *136*, 13925 – 13931; b) C. C. L. McCrory, S. Jung, J. C. Peters, T. F. Jaramillo, *J. Am. Chem. Soc.* **2013**, *135*, 16977 – 16987.
[17] a) G. Mattioli, P. Giannozzi, A. Amore Bonapasta, L. Guidoni, *J. Am. Chem. Soc.* **2013**, *135*, 15353 – 15363; b) J. G. McAlpin, Y. Surendranath, M. Dincă, T. A. Stich, S. A. Stoian, W. H. Casey, D. G. Nocera, R. D. Britt, *J. Am. Chem. Soc.* **2010**, *132*, 6882 – 6883; c) Y. Surendranath, M. W. Kanan, D. G. Nocera, *J. Am. Chem. Soc.* **2010**, *132*, 16501 – 16509.
[18] a) Y. Liu, C. Xiao, M. Lyu, Y. Lin, W. Cai, P. Huang, W. Tong, Y. Zou, Y. Xie, *Angew. Chem. Int. Ed.* **2015**, *54*, 11231 – 11235; *Angew. Chem.* **2015**, *127*, 11383 – 11387; b) Y. Wu, M. Chen, Y. Han, H. Luo, X. Su, M.-T. Zhang, X. Lin, J. Sun, L. Wang, L. Deng, W. Zhang, R. Cao, *Angew. Chem. Int. Ed.* **2015**, *54*, 4870 – 4875; *Angew. Chem.* **2015**, *127*, 4952 – 4957.

Received: November 27, 2015
Revised: December 13, 2015
Published online: January 12, 2016

